Journal of Catalysis 281 (2011) 212–221

Contents lists available at ScienceDirect

Journal of Catalysis

journal homepage: www.elsevier.com/locate/jcat

Oxide clusters as source of the third oxygen atom for the formation of carbonates in alkaline earth dehydrated zeolites

Alexander V. Larin [a,*], Andrey A. Rybakov [a], Georgii M. Zhidomirov [a,b,1], Amber Mace [c], Aatto Laaksonen [c,2], Daniel P. Vercauteren [d,3]

[a] Lomonosov MSU, Moscow, Russia
[b] Boreskov Institute of Catalysis, Novosibirsk, Russia
[c] University of Stockholm, Stockholm, Sweden
[d] University of Namur (FUNDP), Namur, Belgium

ARTICLE INFO

Article history:
Received 8 January 2011
Revised 27 April 2011
Accepted 1 May 2011
Available online 8 June 2011

Keywords:
Carbon dioxide
Carbonate
Alkaline earth zeolites
Density functional theory
Periodic conditions
Infrared spectra

ABSTRACT

In our paper, we show that carbonates can be formed with almost no energetic barrier from CO_2 and metal-oxide binuclear MO_XM species (M = Mg, Ca, Sr, Ba, with X = 1–4, depending on the cation) in alkaline earth zeolites, mordenite (MOR) and phillipsite (PHI), on the basis of quantum mechanical density functional theory (DFT) calculations at both isolated cluster and 3D periodic levels. The participation of MO_XM species (X = 1 and 3) explains the source of the third O atom in CO_3 species in dehydrated zeolites, on the basis of a good agreement between the calculated and experimental positions of the asymmetric and symmetric CO_3 vibration bands, of the ratio of their intensities, and of the weak dependence *versus* the cation and framework type. The reaction of formation of dimethylcarbonate from $CaCO_3Ca$ in the 8-membered (8R) ring of MOR and methanol has also been considered, suggesting the carbonate activity as the source of CO_2 at elevated temperatures.

1. Introduction

The origin of the chemisorbed forms of CO_2 is a key question for modeling its possible chemical mechanisms of activation. In the case of zeolite frameworks, there is, to our best knowledge, still no clear answer about a microscopic model of CO_2 chemisorption for all classes of cation-exchanged zeolite form, involving transition metal, alkaline, and alkaline earth zeolites (AEZ). The CO_2 chemisorbed moiety can correspond to various carbonate species from a negligibly weak coordinated to the strongly coordinated toward one or more zeolite framework atoms. For simplicity, below in the article, we will use the term "carbonate" for all CO_3 moieties independently of their coordination number. Even if numerous assignments of IR spectroscopic data have already been published for those materials [1–6], a final explanation about the carbonate formation remains indeed ambiguous.

Early studies [1,2] mentioned differences between CO_2 adsorbed in the Mg form and in the other AEZ. However, this difference was later denied by the work of Jacobs et al. [3] who registered similar IR bands of carbonates, in particular, in CaX zeolite. The influence of the cation type was shown in Ref. [4] regarding rather moderate variations of the most intense IR band positions. Additionally, weak or at least non-clear dependences of the zeolite framework type (the MgETS-10 zeolite) for similar strong bands manifested at 1620 and 1380 cm^{-1} were noticed in Ref. [6]. A strong doublet at 1665 and 1325 cm^{-1}, conserved in the spectra up to 500 °C, was assigned to carbonate species similar to the one over an MgO surface [7], while a less stable doublet at 1620/1370 cm^{-1} disappears when the temperature rises above 200 °C over MgO. Starting from the assignment available in Ref. [8], the higher and lower frequencies of the CO_3 group were attributed to symmetric and asymmetric carbonate vibrations, respectively [3,4]. A ratio of the higher/lower band intensities was published in Ref. [4]. Going forward, we should note that our assignment of the symmetric and asymmetric carbonate vibrations for the lower and higher branches is inverted *versus* the conventional interpretation [3,4].

An important chemical problem behind our assignment proposed here just above is the origin of the third O atom in the CO_3 species. In hydrated forms, it is obvious that the water oxygen can be involved in the CO_3 formation. For dehydrated zeolites,

* Corresponding author. Fax: +7 495 9384486.
E-mail addresses: nasgo@yandex.ru (A.V. Larin), zhi@catalysis.nsk.su (G.M. Zhidomirov), aatto@mmk.su.se (A. Laaksonen), daniel.vercauteren@fundp.ac.be (D.P. Vercauteren).
[1] Fax: +7 383 3308056.
[2] Fax: +46 8 15 21 87.
[3] Fax: +32 81 725466.

0021-9517/$ - see front matter Crown Copyright © 2011 Published by Elsevier Inc. All rights reserved.
doi:10.1016/j.jcat.2011.05.002

two possibilities were discussed in the literature [3,6]. Either the framework O atoms or the oxo-species can be the source of the third O for the carbonates. On the one hand, the similarity between the various O types denied the suggestion about the participation of the framework oxygens in the carbonate structure [6]. On the other hand, some of us recently considered CO oxidation on binuclear MO_XM clusters ($X = 2–3$) in AEZ at both the isolated cluster [9,10] and periodic [11] calculation levels. It was shown that the products of CO oxidation transform *via* a barrierless reaction profile to carbonates. The present work actually adds evidence for the hypothesis about the oxo-species as the source of O for carbonates. Till now, to our knowledge, no theoretical study proposed a clear explanation of the experimental data obtained so far. The assignment of the carbonate frequencies could thus help to understand the carbonate formation mechanism. The comparison of the IR bands is therefore the main goal of this paper. More precisely, we optimized the structure of the products of the interaction between the MO_XM species (M = Mg, Ca, Sr, Ba, with $X = 1–4$) and CO_2 and calculated the respective frequencies at both the isolated cluster and periodic DFT levels.

2. Computational details

First, we applied the isolated cluster approach, considering Gaussian 03 [12], to check the possibility of carbonate formation over an isolated cation or cluster, as well as to further calculate the frequencies and intensities of the carbonate species in an 8-membered ring (8R) as found in mordenite (MOR) and in a fragment that includes two 6R and 4R windows (6R + 4R) with one common Si–O–Si moiety for zeolite Y. Initial chemical compositions of the cluster models (without carbonate species) are $MAl_2Si_6O_8H_{16}$ and $MAl_2Si_6O_9H_{14}$ for 8R and 6R + 4R, respectively, where M is the AE cation. Two Al atoms are present in both 8R and 6R + 4R models as in our previous work [9–11]. Most of the results were obtained at the B3LYP/6-31G* level, while a higher MP2/6-31G* level was applied in some cases. To determine the reaction coordinate for CO_2 or carbonate reaction with methanol (see Section 4), we applied the QST3 algorithm as supplied with Gaussian 03 considering the optimized geometries of both the reagents and products.

Second, for the periodic approach, we optimized the cell parameters and the geometries of the MO_XM(MOR) and MO_XM(PHI) moieties (M = Mg, Ca, with $X = 1–4$) using VASP [13]. The projector augmented wave (PAW) method [14] was used to describe the electron–ion interactions, and a plane-wave basis set was employed for the valence electrons. The plane-wave cutoff was set to 500 eV. Results were obtained with the PBE and PW91 generalized gradient approximation (GGA) functionals [15]. The Brillouin zone sampling was restricted to the Γ-point. The chemical composition of the unit cell is $MAl_2Si_{46}O_{96}$ for MMOR and $M_2Al_4Si_{12}O_{32}$ for MPHI. The compositions including the MO_XM moieties correspond to $(MO_XM)Al_2Si_{46}O_{96}$ and $(MO_XM)_2Al_4Si_{12}O_{32}$, respectively. The optimized cell parameters are given in Table 1. After optimization of the MO_XM(MOR) moiety, we added CO_2 and performed the optimization of the entire systems. Vibrational frequencies were calculated using the finite difference method as implemented in VASP. Small displacements (0.015 Å) of the atoms from the MCO_3M(MOR) species were used to estimate the numerical Hessian matrix. The rest of the zeolite atoms were kept fixed at their equilibrium positions. As any theoretical approach results in frequency values shifted relative to the experimental data, we scaled all frequencies by fitting one band position ν_{cal} to the experimental ν_{exp} value and then recalculated the positions of the other bands multiplying them by (ν_{exp}/ν_{cal}). Regarding that the frequencies obtained with B3LYP are pretty similar to the experimental ones, we rescaled only the frequencies calculated at the periodic level with PW91. In order to check the accuracy of the projected densities of states (PDOS) of the CaO_3Ca and $CaOCa + O_2$ complexes in MOR, we considered different (2, 2, 2) and (3, 3, 3) sets of shrinking factors. The *s*-, *p*-, and *d*-orbitals for selected Ca, Al, and O atoms were projected in both the singlet and triplet states that possess similar (CaO_3Ca) or essentially different ($CaOCa + O_2$) relative stability. Visualization at both cluster and periodic theoretical levels was realized with the MOLDRAW code [16].

Table 1
Unit cell parameters (*a*, *b*, *c*, in Å, α, β, γ, in degrees) and cell volumes (in Å^3) of MOR and PHI type zeolites as optimized at (PW91) level.

	a	*b*	*c*	α	β	γ	Volume
CaOCa(MOR)	13.73	13.70	15.06	90.33	90.11	83.46	2813.5
CaO_2Ca(MOR)	13.74	13.71	15.08	90.29	90.10	83.36	2821.6
CaO_3Ca(MOR)	13.72	13.67	15.05	90.38	90.10	83.65	2804.9
CaO_4Ca(MOR)	13.70	13.63	15.04	90.44	90.04	85.23	2799.1
MgOMg(MOR)	13.76	13.72	15.11	90.52	89.96	83.49	2834.1
SrOSr(MOR)	13.77	13.74	15.10	90.32	90.07	83.50	2838.7
BaOBa(MOR)	13.78	13.74	15.10	90.28	90.08	83.52	2840.6
MgOMg(PHI)	9.70	13.93	8.90	90.00	124.21	90.00	994.0

3. Results

3.1. Consideration of the framework oxygen for the carbonate formation

To test the possibility of carbonate formation involving a framework oxygen of the zeolite cationic form without any MO_XM species, a series of optimization was performed considering one M cation with both 8R and (6R + 4R) cluster models for all M = Mg, Ca, Sr, and Ba. More precisely, we looked for a geometry in which the carbonate is formed with a third O atom of the framework owing to a partial weakening of its binding to the neighbor T atoms. No carbonate structure could be obtained. Only a linear CO_2 geometry with a maximal distortion of 169.8° was observed for the Mg(8R) cluster in MOR (Fig. 1). The weakness of CO_2 interaction with the framework oxygen in alkali form zeolites was already discussed [17]. The authors concluded as well that carbonate formation should not be observed in regards of the weak interaction between CO_2 and the framework oxygen in this type of zeolites.

3.2. Consideration of the oxygen of metal oxide species for the carbonate formation

3.2.1. Isolated cluster approach

We next studied the reactions between CO_2 and the MO_XM species. The Ca cluster geometries were already described in details

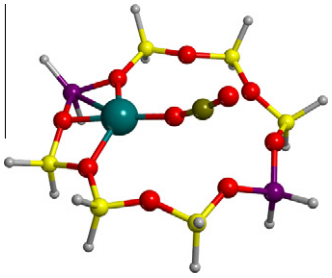

Fig. 1. Optimized structure of the product of CO_2 interaction with the Mg(8R) moiety in MOR, as calculated at the B3LYP/6-31G* level. The color code is O in red, Si in yellow, Al in violet, Ca in blue, C in brown, and H in gray. (For interpretation of the references to color in this figure legend, the reader is referred to the web version of this article.)

[9,10]. The product of the interactions between CO_2 and CaOCa(8R) or BaOBa(8R) as obtained at the B3LYP/6-31G* level is shown in Figs. 2a and b. The positions of the Mg cations and geometries of the MO_XM species were calculated at the cluster and periodic levels, including the carbonate species [11]. We modeled the tetra-dentate carbonate type with three O atoms coordinated toward two M atoms of the MOM cluster. One O is bi-coordinated toward two M atoms, and two others are mono-coordinated toward one M atom (Fig. 2a). Earlier interpretations suggested that mono- and bi-dentate CO_3 groups coordinated to only one cation by either one or two O atoms are presented in zeolites [1–7]. Higher coordination numbers were suggested in alkali zeolites with a higher quantity of monovalent (Na) cations per cell as compared to AEZ, without, however, a respective analysis of the IR spectra [6].

The vibrational frequencies of the carbonate anion were calculated for the isolated $MgCO_3Mg$(6R + 4R) cluster as 1329.5/1645.8 cm^{-1} for the symmetric/asymmetric vibrations (Table 2[4]), respectively, in qualitative agreement with the experimental values, 1734, 1700, 1625, 1382, and 1363 cm^{-1}, assigned to carbonate in MgX [2] as well as with 1620 and 1380 cm^{-1} in MgETS-10 [6]. Similar asymmetric/symmetric doublets were obtained considering other cations (Table 2), thereby confirming a weak dependence of the band positions *versus* the cation type. For the obtained tetra-dentate carbonate structure (Fig. 2a and b), its symmetric vibration is more strongly suppressed and red shifted *versus* the asymmetric one as mentioned over alumina [18]. The tetra-dentate structure allows to find the explanation for the ratio between the intensities of the symmetric and asymmetric vibrations *versus* the usually inverted ones for the respective carbonate vibrations in the gas state.

A tri-dentate structure has been obtained for the products of CO_2 interaction with the CaO_2Ca(8R) (Fig. 2c) and CaO_2Ca(6R + 4R) (Fig. 2d) complexes at the B3LYP/6-31G* level ($X = 2$ in Table 2). The two asymmetric and symmetric vibration bands for the tri-dentate carbonate are shifted to higher, 1869–1960 cm^{-1}, and lower, 1260–1304 cm^{-1}, frequencies *versus* those of the tetra-dentate ones, respectively. Experimentally, it is difficult to register the low-frequency branch of the doublet near 1200 cm^{-1} owing to the intensive framework Si–O–Si vibrations [19]. The high-frequency branch is outside the conventional range from 1800 to 1200 cm^{-1} for carbonates [1–7]. It seems that tri-dentate forms do not appear in most zeolites owing to their lower stability as compared to the tetra-dentate ones obtained with the CaOCa and CaO_3Ca moieties for both (6R + 4R) and 8R type rings. The heats of carbonate formation were calculated, for example, for the CaO_X-Ca(8R) cluster as −72.3 ($X = 1$) and −20.4 ($X = 2$) kcal/mol at the B3LYP level, and as −77.1 ($X = 1$) and −19.9 ($X = 2$) kcal/mol at the MP2 level. The two bands positioned at 1850/1180 cm^{-1} and assigned to the asymmetric/symmetric modes of carbonate, respectively, suggest the presence of a tri-dentate carbonate over an alumina surface [18].

As our computations led to the triplet state as the most stable for the MgO_3Mg(6R + 4R) cluster, the latter was not considered in this study. We considered CO_2 addition to CaO_3Ca(6R + 4R) only. We observed the formation of the tetra-dentate $CaCO_3Ca$(6R + 4R) carbonate, *i.e.*, the product of CO_2 addition to CaOCa(6R + 4R), and simultaneously the formation of an O_2 fragment coordinated to the upper Ca cation.

The stability of metal-oxide binuclear MO_XM species was confirmed experimentally for M = Ga [20], while it was considered as doubtful for ZnOZn on the basis of computational results [21]. Not knowing any discussion regarding the AEZ MO_XM species, we have recently evaluated the reactions of their formation at

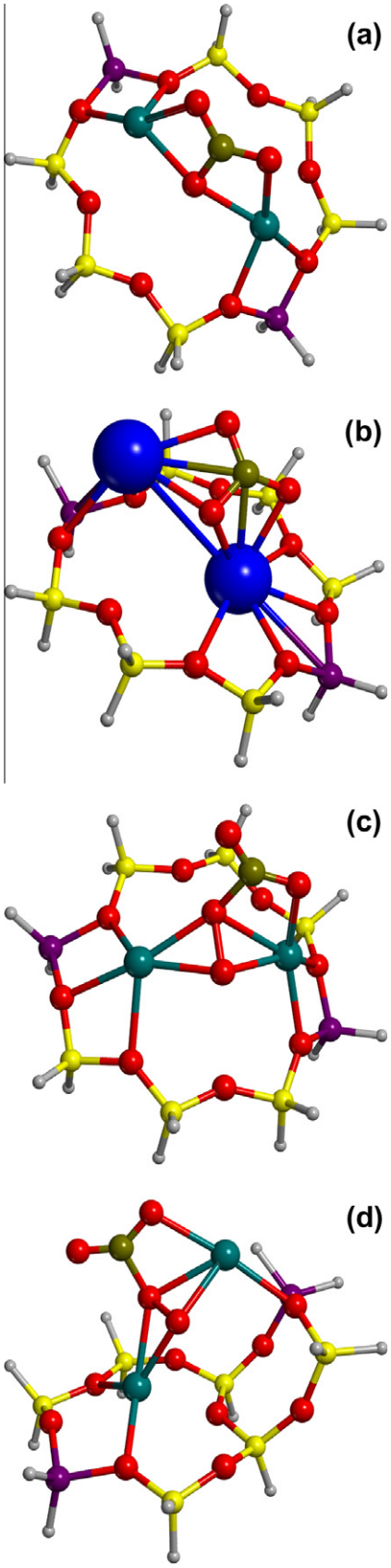

Fig. 2. Optimized structures of the products of CO_2 interaction with the CaO_XCa(8R) (a: $X = 1$ and c: $X = 2$) moieties in MOR, (b) BaOBa(8R) moieties in MOR, and (d) CaO_2Ca(6R + 4R) moieties in FAU, as calculated at the B3LYP/6-31G* level. The color code is the same as in Fig. 1, Ba in light blue. (For interpretation of the references to color in this figure legend, the reader is referred to the web version of this article.)

[4] For shortness in Table 2, we compare the experimental data for CaX from Ref. [4] keeping in mind the similarity between the X and ETS-10 zeolite framework types and the cationic forms.

Table 2
Band positions (cm^{-1}) of the asymmetric (ν_{asym}) and symmetric (ν_{sym}) vibrations as well as the intensity ratios (I_{asym}/I_{sym}) for the carbonate species in the MO_XM(6R+4R) cluster (M = Mg, Ca, Sr, Ba) calculated at the B3LYP/6-31G* level compared to the experimental data for X = 1 [4] and X = 2 [18].

	Mg	Ca	Sr	Ba	Experiment
X = 1					
ν_{asym}	1645.8	1664.0	1663.0	1651.0	1700, 1665, 1625[a]
ν_{sym}	1329.5	1333.7	1335.9	1342.6	1365, 1390, 1440[a]
I_{asym}/I_{sym}	1.24	1.62	1.37	1.37	1.45–1.55[a]
X = 2					
ν_{asym}	1912.0	1959.7	1874.7	1868.7	1850[b]
ν_{sym}	1260.0	1267.7	1279.3	1303.5	1180[b]
I_{asym}/I_{sym}	1.16	1.31	1.47	2.50	–

[a] Upper ν_{asym} and lower ν_{sym} values correspond to the three doublets in CaX zeolite [4].
[b] For alumina [18].

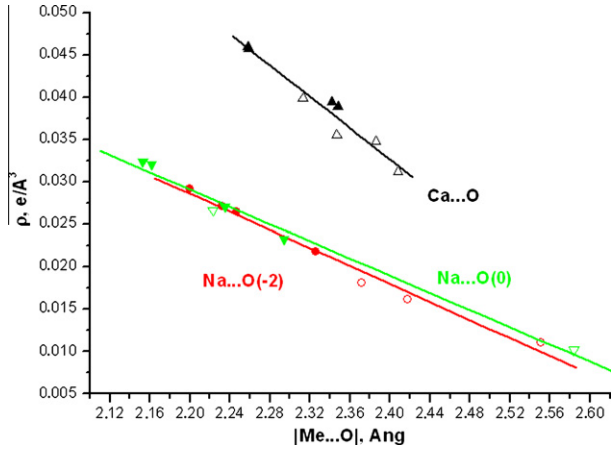

Fig. 3. Electron densities ($e \times Å^{-3}$) at the critical points between the Na (triangles down) or Ca (triangles up) cations and the zeolite framework (open symbols) or carbonate (closed symbols) oxygens *versus* the M···O distance (Å) calculated in the neutral (Na···O(0)) or charged (Na···O(-2)) 6R + 4R and 8R clusters, respectively, at the MP2/6-31G* level.

the cluster [9,10] and periodic [11] levels as exothermic. The formation of the carbonates can serve as a confirmation of the presence of metal-oxide binuclear MO_XM species in the AEZ forms. Such explanation can be confirmed *via* the comparison of the electron densities (ED) at the bond critical points (CPs) between the cations and the framework O_{zeo} or carbonate O_{carb} oxygens. The ED difference illustrates the relative strength of the bonds. Would the bond M–O_{carb} be stronger than the M–O_{zeo} one, then we could admit that carbonate is not anchored to the framework and hence could move together with one or two cations. In such a way, carbonate could gradually trap the first cation and then, after a drift, trap the second one. To elucidate this possibility, we calculated the CPs and ED values using Bader AIM theory [22] as supplied with the Gaussian code.[5] The ED difference at the M–O_{carb} (Fig. 3, closed triangles) and M–O_{zeo} (Fig. 3, open triangles) bonds is rather small to justify such model. Hence, we cannot approve the mobility of the carbonate species in the AEZ lattice. For comparison, this last conclusion does not suit for carbonates with alkali cations. The difference between the EDs of the Na–O_{carb} and Na–O_{zeo} bonds is also emphasized (Fig. 3, open and closed circles), similarly for lower ED values relative to the ones that obtained for the AEZ carbonates. The lower potassium bonding with the framework results in a higher cation mobility together with the carbonates, as found experimentally [24–26] and interpreted for the mixed NaKA zeolite [23]. It also signifies that the AEZ carbonate formation can happen at two AEZ cations that are closely located as parts of the binuclear MO_XM species. That is why we consider the AEZ carbonate formation as the indirect confirmation of the MO_XM presence in AEZ. Mixed earth alkaline (M)–alkali (M′) carbonates (MCO_3M') are also immobile in the zeolites. Such species appear, for example, in the course of partial sodium exchange and present similar vibrational spectra [27].

3.2.2. Periodic approach

3.2.2.1. Heat of formation and favored multiplicity of the MO_XM species at the periodic computational level.

3.2.2.1.1. CaO_XCa species in mordenite (MOR). In order to model the carbonate formation, we needed to determine the ground state of each of the considered systems. Structural and energetic aspects at the isolated cluster computational level have already been presented [9–11]. The favored multiplicity of each CaO_XCa species was determined by the sign of the ΔU_{ST} difference between the total energies of the singlet and triplet states ($\Delta U_{ST} = U_S - U_T$), a positive value corresponding to a favored triplet state (Table 3). The signs of the ΔU_{ST} values vary with X. We remind that at the cluster level, ΔU_{ST} was negative for Ca for any X = 1–4 values,[6] while ΔU_{ST} was negative for Mg for X = 1–2 only. For Sr and Ba, an intermediate situation was observed, *i.e.*, $\Delta U_{ST} < 0$ for X = 1–3. Herein, we additionally discuss for the first time the favored multiplicity of the CaO_XCa species in zeolites at the periodic computational level.

One of the sharp differences between the cluster and periodic models resides in the respective ΔU_{ST} values (Table 3). A non-correct estimation is obtained at the cluster level for the triplet CaOCa(8R) moiety only. The exaggerated ΔU_{ST}^{CL} difference between the singlet and triplet energies at the cluster level (−118.0 kcal/mol with MP2) relative to the periodic values (−0.39 and −0.30 kcal/mol with PW91 and PBE, respectively) is the result of a strong distortion of the triplet CaOCa(8R) moiety and of the localization of the spin density at the capping H atom. The maximal spin density is concentrated at the capping H atom (0.916 *e*) closest to the Ca cation (0.916 *e*) that is detached from the O atoms of the 8R ring (Fig. 4a). Only a minor spin density (0.105 *e*) is concentrated at the second Ca cation of the Ca–O–Ca bridge. It is a rare case when the computations of the electron correlation at the MP2 level result in a worse ΔU_{ST}^{CL} as compared to DFT. For comparison, calculations with B3LYP do not shift the spin density to the capping H atom and give ΔU_{ST}^{CL} = −55.8 kcal/mol. We did not include the triplet CaOCa(6R + 4R) cluster case in Table 3, but MP2 also resulted in an exaggerated ΔU_{ST}^{CL} difference of −134.4 kcal/mol. In this last case, the bond of the capping H atom near Al is strongly elongated (isolated H atom in the lower left corner of Fig. 4d) so that Al becomes tricoordinated. And again, the triplet CaOCa(6R + 4R) cluster presents normal lengths of all T–H bonds (T = Al, Si), when optimized using B3LYP (Fig. 4d). The problem of the triplet MO_XM distorted geometry obtained at the MP2 level, however, disappears with higher X values. For the triplet CaO_2Ca(8R) already, the spin density is only concentrated on the oxygen atoms (1.032 *e*) that do not form an O–O bond, whereas minor density values correspond to the Ca cations (both −0.040 *e*). The difference between the singlet and triplet geometries of CaO_2Ca(8R) resembles to the geometries of the CuO_2-Cu models [6,7] with one O–O bond present in one of them, (μ–η^2:η^2-peroxo)dicopper, only.

[5] The ED values in Fig. 3 are given for charged $NaCO_3Na(6R + 4R)^{2-}$ cluster but similar ED differences remain if one uses neutral and all-siliceous 6R + 4R clusters. For the neutral case (with two H atoms in the 6R + 4R cluster), the higher mobility of the sodium carbonate results in its displacement towards one O atom of the carbonate coordinated to one of the protons in the 6R. The ED comparison is therefore not straightforward. More details about the Na clusters are given in Ref. [23].

[6] For X = 4, no ΔU_{ST} was calculated but the singlet state is stable as compared to the triplet one for which no convergence was achieved.

Table 3
Relative and absolute energies (eV) of the singlet (U_S) and triplet (U_T) states of the O_2 molecule as well as of the MOR and PHI unit cells including the CaO_XCa and MgO_XMg species, singlet–triplet energy differences ($\Delta U_{ST} = U_S - U_T$, kcal/mol), ΔU_{ST}^{CL} (kcal/mol) at the B3LYP and PW91 levels of the isolated 8R cluster [9–11], and heats ΔU of the reaction (1)[a] (kcal/mol) between singlet states using VASP (PW91).

Species	U_S PW91	U_T PW91	ΔU_{ST} PW91	ΔU_{ST} PBE	ΔU_{ST}^{CL} PW91	ΔU_{ST}^{CL} B3LYP	ΔU
O_2	−8.750	−9.766	23.65	25.14	41.37	33.12	–
MOR							
CaOCa	−1160.064	−1160.047	−0.39	−0.30	–[c]	−55.8, −118.0[b]	–
CaO_2Ca	−1165.561	−1165.545	−0.37	−0.27	−26.2	−31.2, −41.9[b]	−14.04
CaO_3Ca	−1170.389	−1170.409	0.46	0.31	−21.1	−14.2	1.38
$CaOCa + O_2$	−1168.987	−1169.361	8.62	10.00	–	–	19.67
CaO_4Ca	−1175.721	−1175.722	0.02	0.06	−8.4	–[c]	−10.23
PHI[d]							
MgOMg	−403.543	−403.544	0.01	0.00	–	–[c]	–
MgO_2Mg	−413.710	−413.711	0.01	0.01	–	–[c], −43.5[b]	−4.51
MgO_3Mg	−422.571	−422.570	−0.01	0.00	–	9.9, 10.2[b]	10.55
$MgOMg + O_2$	−422.734	−423.334[e]	6.92	8.24	–	–	4.17
MgO_4Mg	−431.407	−431.410	0.03	0.04	–	19.6	10.84
$MgO_2Mg + O_2$	−432.491	−433.701[e]	13.95	14.67	–	–	8.89

[a] the steps for reaction (1) at $X = 2$–4 for Ca are illustrated in Fig. 6.
[b] MP2/6-31G* level.
[c] no SCF convergence while using B3LYP/6-31G* for triplet states.
[d] the energy corresponds to two MgO_XMg species per PHI cell, so that the ΔU_{ST} and ΔU values are divided per two.
[e] for non-symmetric cell (P1 group).

The energy difference between the singlet and triplet MO_XM states disappears while going from the cluster calculations to the periodic models using VASP for the MOR or PHI zeolites (Table 3). It can be confirmed by comparison between the projected densities of states (PDOS) of the singlet and of the triplet states of similar atoms in the different systems. For example in Fig. 5a, we compare the PDOS of the sum of the up and down spin states at the O97 atom, the side atom in the CaO_3Ca moiety, to the total PDOS value of the singlet CaO_3Ca species for MOR (right lower corner in Fig. 6), for which the energies of the triplet and singlet CaO_3Ca moieties are pretty close (0.46 kcal/mol at the periodic PW91 level, Table 3). The difference between the PDOS values is minor for all the Ca, O, and Al atoms.[7] On the opposite, a sharper difference is noted between the PDOS values on the O97 atom in the singlet and triplet states of the Ca–O97–Ca + O_2 system (Fig. 5b) which is more stable in the triplet state by 8.62 kcal/mol than in the singlet one at the periodic PW91 level (Table 3).

Two cases of a decrease in the energy differences ΔU_{ST} between the singlet and triplet complexes containing O_2 species were already discussed in the literature [28,29]. The precise value of the small ΔU_{ST} separation calculated using the MR-CISD method for the Li^+O_2 complex is difficult to evaluate from the illustration in Ref. [28]. The molecular HO_2^+ cation is much better characterized by a rich series of accurate theoretical approaches, with a ΔU_{ST} value around 4.45 ± 0.15 kcal/mol [29], a much smaller value relative to the one for the O_2 gas state (from 23.65 to 41.37 kcal/mol in upper line of Table 3).

To our best knowledge, only the MO_XM clusters with $X > 2$ are suspected as the centers that can accumulate $^1O_2$ in various zeolites [28]. The stability of the singlet state (even if with a minor advantage of the triplet state) is in agreement with the fact that a singlet oxygen can thus be desorbed *via* a spin-allowed channel from the ^1MO_XM to the $^1MO_{X\text{-}N}M$ cluster while loosing $^1O_2$. Namely, this fact justifies our initial idea about the treatment of the singlet MO_XM clusters only [9,10]. The experimental facts prove that AEZ types also easily trap triplet oxygen [30], which then can oxidize organics under thermal stimulation without additional source of oxygen. The last authors paid attention that the oxidation of propane takes place only after a preliminary treatment in air/oxygen atmosphere. But if the relatively easy $^1O_2$ yield in AEZ obeys to spin conservation, then the $^3O_2$ trapping reaction has to be also a spin-allowed process [30]. It suggests that the product of the ^1MO_XM reaction with $^3O_2$ has to possess a triplet $^3MO_{X+2}M$ state in order to allow the $^3O_2$ trapping. The closeness in energy and geometries between $^1MO_{X+2}M$ and $^3MO_{X+2}M$ permits a fast transition from triplet $^3MO_{X+2}M$ to singlet $^1MO_{X+2}M$. The similarities between the triplet and singlet energies make less crucial the problem of the exact spin determination in the ground state. This question of spin distribution in zeolites seems to be directly related to the locally non-compensated charge distributions discussed recently [31]. Tentatively, the energies vary relatively slightly at the periodic level when the compensating cation or the GaO_XGa species located far from the substituting Al atom [31]. The problem of the closeness between the different multiplet states remains an interesting point for a future research requiring a powerful electron correlation method at the periodic level.

The low absolute ΔU_{ST} values allow to check the thermodynamic possibility of the consequent oxidation steps between the singlet or triplet $CaO_{X-1}Ca$ and CaO_XCa species ($X = 1$–4) at the periodic level as it was done at the cluster level [9,10]. For example, for the reaction between the singlet states as we discussed before [9–11]:

$$^1MO_{X-1}M + 1/2\,^3O_2 \rightarrow {}^1MO_XM \qquad (1)$$

we got, for all X values and M = Ca, an exothermic ΔU energy with the exception of $X = 3$, for which we got an endothermic effect of 1.38 kcal/mol (Table 3 and Fig. 6). For the reaction $^1CaOCa(MOR) + {}^3O_2 \rightarrow {}^1CaO_3Ca(MOR)$, we observed an exothermic heat of (−14.04 + 1.38) = −12.66 kcal/mol (Fig. 6). Hence, all the CaO_XCa species for $X = 1$–4 can be obtained and can react with CO_2, as analyzed below.

3.2.2.1.2. MgO_XMg species in phillipsite (PHI). Even if the 8R window looks more distorted in PHI *versus* the one in the cluster 8R model (see Fig. 1 of [11]), the angles and distances in the MgO_2Mg moiety are nearly the same for both MgO_2Mg(PHI) and MgO_2Mg(8R)

[7] We added the Al atoms in the comparison because they are differently located around the MO_XM species in the MOR and PHI frameworks (Fig. 7). Hence, Al atoms could be responsible for the difference between the signs of the ΔU_{ST} values between the MOR and PHI cases for $X = 1$ or 2 at the periodic level. But they do not share the spin densities in both the cases.

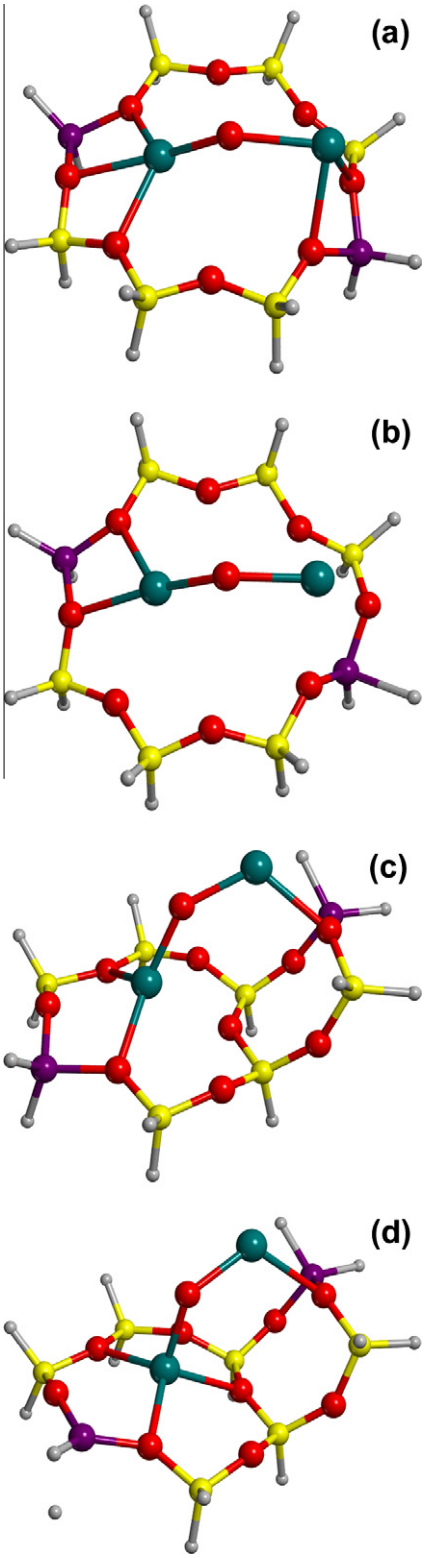

Fig. 4. Optimized structures of the triplet CaOCa moieties in the (a and b) 8R and (c and d) 6R + 4R clusters, respectively, as obtained at the (a and c) B3LYP/6-31G* and (b and d) MP2/6-31G* levels. The color code is the same as in Fig. 1. (For interpretation of the references to color in this figure legend, the reader is referred to the web version of this article.)

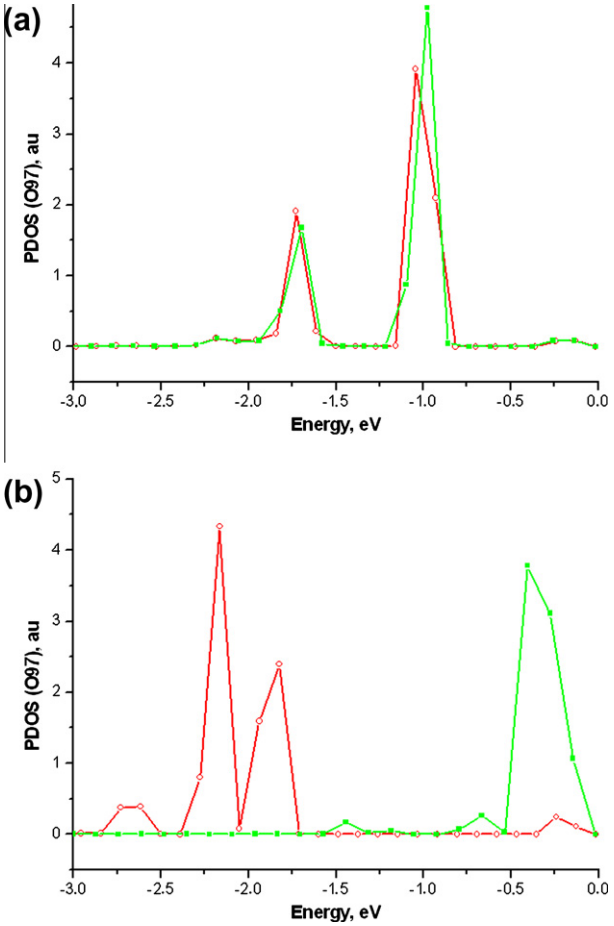

Fig. 5. Projected spin densities of the singlet (open symbols) or triplet (closed symbols) states (PDOS) regarding the *p*-orbitals of the side O97 (a) atom in the O_3 fragment of the singlet or triplet CaO_3Ca state and (b) in the Ca–O97–Ca fragment in the singlet or triplet $CaOCa + O_2$ states in MOR. The Fermi energy corresponds to zero. The location of the O97 atom in CaO_3Ca is shown in Fig. 6.

complexes. Details about their geometries are given in Ref. [11]. In this last paper, it was shown that MgO_XMg clusters possess a ground singlet state for $X = 1–2$ and a ground triplet one for $X = 3–4$ at the level of the isolated 8R (Table 3 of Ref. [11]) and 6R + 4R clusters.[8] The ΔU_{ST} values for $X = 1–2$ could not be calculated at the B3LYP level because SCF convergence could not be achieved for both triplet states with $X = 1–2$ for the isolated 8R and 6R + 4R clusters. This non-convergence for the triplet states can also be considered as an evidence of their instability. At the MP2 level, the ΔU_{ST} values are negative for $X = 1–2$, manifesting the favored singlet state. Let us add that the ΔU_{ST} signs coincide at both MP2 and B3LYP levels as shown earlier for Ca clusters [10].

Regarding the periodic results, we got a negative $\Delta U = -9.01$ kcal/mol/cell[9] value for $X = 2$, thus suggesting the thermodynamic possibility of the MgO_2Mg formation at the periodic level *via* the same reaction equation as Eq. (1). The ΔU_{ST} difference is indeed very small for MgOMg and MgO_2Mg, suggesting clearly that the MgO_XMg species in singlet states can interact with CO_2 and form carbonates. All the carbonate species studied herein possess a singlet electronic ground state. Hence, their formation is not forbidden owing to the change of the total spin in the course of the interaction between MgO_XMg and CO_2. The results of periodic calculations (Table 3) show that the MgO_3Mg and MgO_4Mg moieties are characterized by positive ΔU values, *i.e.*, 21.10 and 21.68 kcal/mol/cell, respectively, so

[8] The ΔU_{ST} sign used in this present paper is inverted *versus* the one adopted in Refs. [9–11].

[9] −4.62 kcal/mol (Table 2) or −9.24 kcal/mol/cell = (−413.710 + 403.543 + 9.766) × 23.05 regarding two MgO_XMg species per cell.

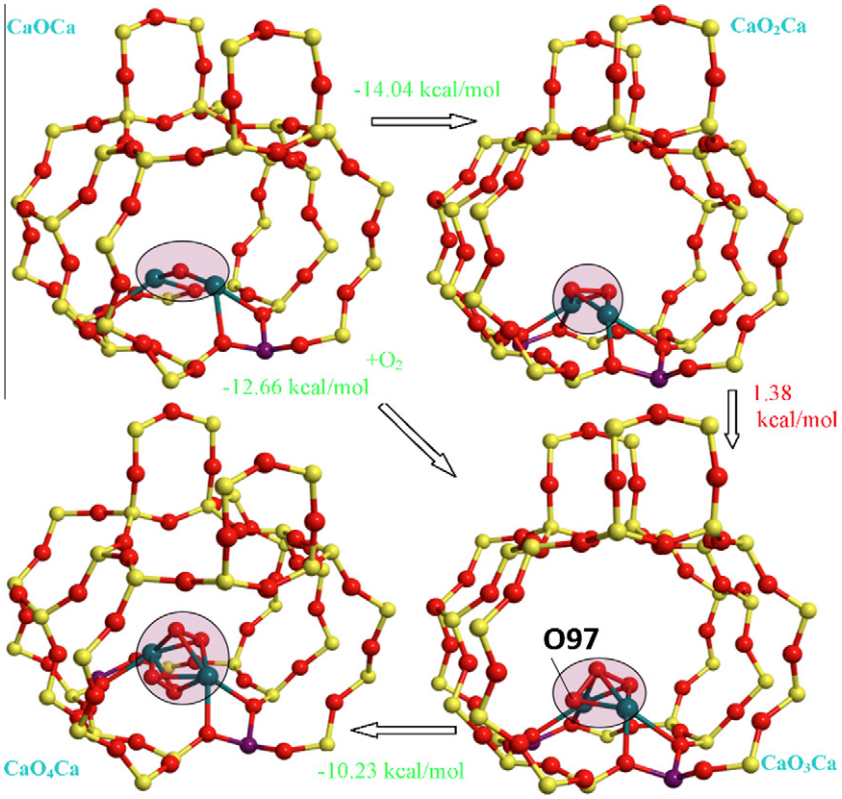

Fig. 6. Optimized structures of the CaO_XCa clusters ($X = 1–4$) in MOR and heats of the $CaO_{X-1}Ca + ½^3O_2 \rightarrow CaO_XCa$ reactions (kcal/mol) as calculated at the PDFT/PW91 level with VASP. The CaO_XCa moieties are shown by the ellipses. The color code is the same as in Fig. 1. (For interpretation of the references to color in this figure legend, the reader is referred to the web version of this article.)

that they are forbidden from thermodynamic point of view. Moreover, both MgO_3Mg and MgO_4Mg species are less stable than the $MgO_XMg + O_2$ pairs for $X = 1$ or 2, respectively, and thus have to decompose.

The oxidation activity of Mg type zeolites can be related with the MgO_2Mg formation. We also therefore considered the inverse reaction of the loss of singlet oxygen:

$$^1MO_2M \rightarrow {}^1MOM + 1/2^1O_2 \quad (2)$$

Singlet and triplet states are even more closer in energies for both MgOMg and MgO_2Mg species in PHI than for the Ca analogs in MOR. We can thus admit that the reaction of oxygen trapping (3) is also spin allowed in MgPHI followed by a triplet to singlet transformation (4) owing to the similar geometry and energy:

$$^1MOM + 1/2^3O_2 \rightarrow {}^3MO_2M \quad (3)$$

$$^3MO_2M \rightarrow {}^1MO_2M \quad (4)$$

The reasons for the smaller ΔU_{ST} energies in PHI relative to the ones in MOR remain non-clear. The comparison of the spin distributions in MOR and PHI did not show any Al participation which is symmetric and asymmetric in the MOR and PHI zeolites, respectively, near the MO_XM species. A partial answer about the possible role of the cation was obtained using analogous ΔU_{ST} calculations in MgMOR. The ΔU_{ST} energies are smaller than ΔU_{ST} for CaMOR and are similar to the ones for MgPHI (Table 4). Hence, the selection of the cation is important for the absolute ΔU_{ST} value. Let us note that this difference is, however, smaller than the precision of the calculations.

We can thus finally explain the oxidation activity of the Mg form zeolites by the MgO_2Mg formation as already shown for the series of Ca clusters regarding the Ca forms [9,10]. The specific property of the Mg forms relative to carbonate formation in the other AEZs is determined by the lower activation barrier of the chemisorption complex (15.3 kcal/mol) for CO oxidation obtained at the periodic level [11]. Such a complex was also optimized for the Zn forms with an activation energy of 23.6 kcal/mol at the cluster level [9]. For the other AEZs, we did not obtain a similar chemisorption complex, leading to the decrease in the activation energy.

Table 4
Relative and absolute energies (eV) of the singlet (U_S) and triplet (U_T) states of the MOR unit cell including the MgO_XMg species, singlet–triplet energy differences ($\Delta U_{ST} = U_S - U_T$, kcal/mol), and ΔU heats for reaction (1) (kcal/mol) between singlet states using VASP (PW91) level.

Species	U_S	U_T	ΔU_{ST}	ΔU
MgOMg	−1157.017	−1157.014	−0.07	–
MgO_2Mg	−1162.393	−1162.392	−0.02	−14.04

3.2.2.2. CO_2 interaction with the MO_XM(MOR) species. The geometries of the carbonate anions regarding CO_2 addition to the MO_XM(MOR) reagents (M = Mg, Ca) were calculated at the periodic level using VASP [13] for the M forms of mordenite (MMOR) and the M forms of phillipsite (MPHI). The oxidation reaction sequence regarding the CaO_XCa(MOR) reagent structures from $X = 1$ to 4 as optimized at the periodic level is presented in Fig. 6 and Table 3. The MO_XM geometries obtained at the periodic level are pretty similar to the cluster ones obtained with B3LYP/6-31G* [9–11].

Regarding the CO_2 adsorption over the CaOCa(MOR) and $CaCO_3Ca$(MOR) species, we obtained stable 3D structures with two frequencies with low absolute values, 1587.4 and 1255.4 cm^{-1}, relative to 1648.8 and 1346.7 cm^{-1} for the 8R cluster

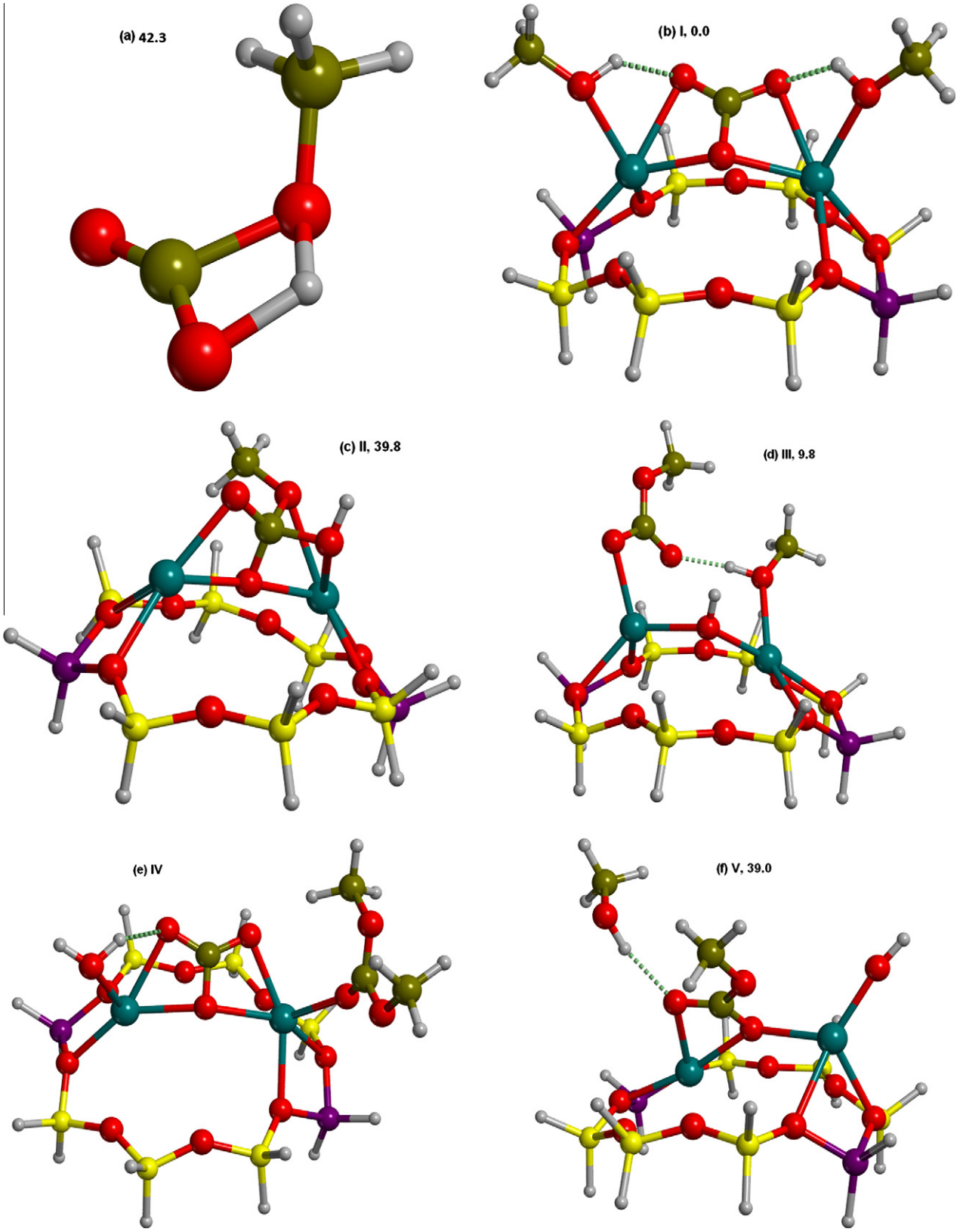

Fig. 7. Optimized structures in the gas state: of the (a) transition state (the structures of the reagents and product in the gas state are simple and omitted for shortness), in the zeolite using $CaCO_3Ca(8R)$ moieties as source of CO_2: of the (b) reagents, (c and f) intermediate states, and (d and e) products for the reaction between CO_2 and CH_3OH obtained at the B3LYP/6-31G* level. The color code is the same as in Fig. 1. The relative energies (kcal/mol) are shown for the different steps of the same brutto chemical composition. Hydrogen bonds are shown by dotted lines. (For interpretation of the references to color in this figure legend, the reader is referred to the web version of this article.)

model of MOR. Also, as mentioned above, any result coming from a theoretical approach leads to frequency values shifted relative to the experimental data; hence, we rescaled the calculated periodic PW91 values as the most strongly displaced ones relative to the experimental data. Fitting the symmetric vibration of 1255.4 cm^{-1} to the "cluster" value of 1346.7 cm^{-1}, instead of 1587.4 cm^{-1}, we got a rescaled[10] asymmetric vibration of 1666.8 cm^{-1} to be compared with the 8R cluster value of 1648.8 cm^{-1} for MOR or the (6R + 4R) cluster value of 1664.0 cm^{-1} for FAU (Table 2).

Regarding the interaction between the MO_2M homologues and CO_2 at the periodic level, we did not succeed to obtain tri-dentate carbonate species as the ones optimized at the cluster level for MOR or FAU (Fig. 2c and d). At the periodic level, we did not get any product of interaction between MO_2M and CO_2 neither for MOR nor for PHI. We consider this as a confirmation that tri-dentate species (Fig. 2c and d) do not appear in the AEZ forms. As well, it is indirectly confirmed by the absence of an upper frequency branch for the chemisorbed species, *i.e.,* as calculated between 1860 and 1960 cm^{-1} ($X = 2$ in Table 2), in the experimental spectra of AEZ.

Similarly, we did not get any tri-dentate carbonate species *via* the periodic study for the interaction between CO_2 and the MO_3M homologs. In this respect, the periodic model of CO_2 adsorption over CaO_3Ca(MOR) species totally confirms the results of the cluster computations. The periodic model also led to the formation of an O_2 fragment separated from $CaCO_3Ca$(MOR) with bands at 1516.8 and 1225.5 cm^{-1}. Rescaling the 1225.5 cm^{-1} periodic value to the "cluster" one of 1346.7 cm^{-1}, we got, instead of 1516.8 cm^{-1}, a rescaled value[11] of 1702.8 cm^{-1} to be compared with the 8R cluster value of 1648.8 cm^{-1} for MOR or the (6R + 4R) cluster one of 1664.0 cm^{-1} for FAU (Table 2).

4. Carbonate step in CO_2 activation

The relevance to consider the studied MCO_3M systems toward the catalytic problems of CO_2 capture and reactivity can be discussed from many points of view. The most important one is the knowledge of a complete set of reactive sites that can be involved in the analyses of a selected process in cationic form zeolites. As we have mentioned above (see Section 3.2.1), the presence of the carbonate species proves the existence of active MO_XM binuclear clusters in the AEZ forms. The MCO_3M carbonates are fixed in the zeolite framework and do not move so that AEZ carbonate can appear when a MO_XM binuclear cluster exists already in the zeolite. The second additional advantage of the presented cluster moieties as potent catalytic system is the relation between the coordination number, three or four, of the carbonate and their IR spectra. The higher the energy difference between the low- and high-frequency branches, the closer the carbonate to the tri-dentate type. Similar coordinations could thus be proposed when doublets will be observed for a new zeolite system based on the doublet splitting. Third, it is clear that carbonate species can participate in many catalytic processes that include CO_2 binding. Such example can be shortly discussed keeping the main emphasis on the carbonate presence in the zeolites and their properties.

We considered the interaction between methanol and CO_2, suggesting a similar activity for CaY as compared to CuY at elevated temperatures [32]. A gas-phase reaction can be proposed *via* a proton transfer step toward CO_2 with a heat of endothermic CH_3HCO_3 formation evaluated as 11.5 kcal/mol at the same B3LYP/6-31G* levels as was applied above in our work for the carbonate calculations. The activation energy in the gas phase is 42.3 kcal/mol, and the imaginary frequency is 1699*i* cm^{-1} in the transition state (Fig. 7a). The favored orientation of CO_2 and CH_3OH is determined by electrostatic interactions between the CO_2 quadrupole and CH_3OH dipole so that the orientation is deeper by around of 1.3 kcal/mol than the O═C═O···H—OCH_3 geometry with hydrogen bonding.

The same reaction with methanol was repeated as in the gas phase but introducing the $CaCO_3Ca$(8R) carbonate into the reactions instead of the gas-phase CO_2 molecule. The relevance of the Ca carbonate for the reaction can be confirmed by a slight exothermic effect of −3.7 kcal/mol if one estimates the energy of the reagents involving the initial structure I (Fig. 7b) and final product IV (Fig. 7e). The energy of the reagent corresponds to the sum of the energy of the optimized structure I (Fig. 7b) containing two CH_3OH molecules and the energy of an isolated CO_2 molecule at the same B3LYP/6-31G* level. The energy of the product IV (Fig. 7e) corresponds to the formation of dimethylcarbonate *via* a barrierless reaction with CO_2, which restores the $CaCO_3Ca$(8R) carbonate and hence completes the catalytic cycle. We will discuss only the first step of the reaction that leads to the $CH_3CO_3^-$ anion formation as part of the complex III (5). Fig. 7 includes the energy values for all the models (Figs. 7b–d, f) with a similar chemical composition (with the exception of product IV that presents a two-step carbonylation as described above). The endothermic effect of the one-step reaction is smaller, 9.8 kcal/mol between structures I and III (Fig. 7d), relative to the gas phase, 11.5 kcal/mol. However, we did not get the transition state (TS) that corresponds to the O-H breaking in methanol as in the gas-phase reaction. We obtained two intermediates II (Fig. 7c) and V (Fig. 7f) with energies lower than 40 kcal/mol, hence smaller than the activation energy in the gas phase (42.3 kcal/mol). It is very interesting to note that the carbon geometry in state II corresponds to a sp^3 hybridization while it is usually sp^2 in the initial and final CO_3 states. Both the II and V states can serve to look for the TS *via* the following mechanism as first step of dimethylcarbonate formation:

$$\begin{aligned} CaCO_3Ca(8R) + 2CH_3OH &\rightarrow Ca(CH_3O\cdots CO_3H)Ca(8R)\cdots HOCH_3(II, V) \\ &\rightarrow HO{-}Ca(CH_3CO_3)Ca(8R)\cdots HOCH_3(III) \\ &\rightarrow CH_3HCO_3 + CaOCa(8R)\cdots HOCH_3 \end{aligned} \quad (5)$$

The state II is especially promising as initial point for the proton transfer. However, the problem of localization of the TS at the cluster level met an obstacle created by the bending vibrations of the capping hydrogens of the 8R cluster. Owing to the fixed H atoms, the Si–H and Al–H frequencies are also imaginary. The reaction coordinate for the first step of dimethylcarbonate formation involves the motions of both the CH_3O and OH groups that should result in a low imaginary frequency. We thus obtained a series of vibrations with imaginary frequencies below 400*i* cm^{-1} in which the contribution of the motion along the coordinate of methanol decomposition is relatively weak. We believe that calculations based on the use of periodic models could avoid this problem of the TS search with an activation energy lower than 40 kcal/mol. Such work is in progress. Nevertheless, the initial modeling step shows thus a perspective of carbonate inclusion into the reaction schemes for CO_2 binding and activation in AEZ type zeolites.

5. Conclusions

Using cluster and periodic type DFT calculations, we demonstrated a clear correspondence between the experimental IR band positions and those calculated for tetra-dentate carbonate species between two cations within the MO_XM type species (M = Mg, Ca, Sr, Ba, with $X = 1$–4) present in alkaline earth dehydrated zeolites. The frequencies of the theoretically obtained rigid MCO_3M

[10] (1346.7/1225.5) × 1516.8 = 1666.8 cm^{-1}.
[11] (1346.7/1255.4) × 1587.4 = 1702.8 cm^{-1}.

structure remain nearly invariant *versus* the type of M cation or the type of framework in agreement with numerous experiments [1–7]. Our models allow explaining the experimental intensity ratio [4] of the two bands presented in Table 2. In all cases, the higher frequency, *i.e.*, 1600–1700 cm^{-1}, corresponds to asymmetric carbonate vibrations, while the asymmetric/symmetric intensities result in comparable ratio *versus* the experimental ones. Two bands of asymmetric and symmetric vibrations for tri-dentate CO_3 with $X = 2$ are outside the conventional range between 1800 and 1200 cm^{-1} for carbonates [1–7]. Tri-dentate forms (Fig. 2c and d) do not appear in most of zeolite forms owing to their lower stability *versus* the tetra-dentate ones [9,10]. Our present work thus confirms that oxo-species serve as the source of oxygen for carbonate formation. Reactions including interaction between oxo-species and other small molecules will also be important at normal or high temperature conditions and need to be elucidated. Theoretical studies regarding such reactions are under progress. Our first results here presented relative to dimethylcarbonate formation with the $CaCO_3Ca$ carbonate as source of CO_2 demonstrate various intermediate states that can be considered as good initial points for the search of the transition states for reactions between carbonates and methanol under moderate temperatures.

Acknowledgments

The authors thank the FUNDP, the FNRS-FRFC, and the Loterie Nationale (convention 2.4578.02) for the use of the Namur Interuniversity Scientific Computing Facility (ISCF) Centre. The authors are extremely grateful to the Computer Complex SKIF of the Lomonosov Moscow State University "Chebyshev" for the computational time and to his manager, Dr. S.A. Zhumatii, for his help. A.A.R. and A.V.L. thank the FNRS and WBI for their stays at the FUNDP. The authors also acknowledge the WBI for financial support in the framework of the «Programme de coopération 2008–2010 entre la Communauté française de Belgique, la Région wallonne et la Fédération de Russie» (convention 2008/18342).

References

[1] L. Bertsch, H.W. Habgood, J. Phys. Chem. 67 (1963) 1621.
[2] J.W. Ward, H.W. Habgood, J. Phys. Chem. 70 (1966) 1178.
[3] P.A. Jacobs, F.H. van Cauwelaert, E.F. Vansant, J.B. Uytterhoeven, J. Chem. Soc., Faraday Trans. I 69 (1973) 1056.
[4] P.A. Jacobs, F.H. van Cauwelaert, E.F. Vansant, J. Chem. Soc., Faraday Trans. I 69 (1973) 2130.
[5] G. Martra, S. Coluccia, P. Davit, E. Gianotti, L. Marchese, H. Tsuji, H. Hattori, Res. Chem. Intermed. 25 (1999) 77.
[6] F.X. Llabrers i Xamena, A. Zecchina, Phys. Chem. Chem. Phys. 4 (2002) 1978.
[7] J.V. Evans, T.L. Whateley, Trans. Faraday Soc. 63 (1967) 2769.
[8] L.H. Little, Infrared Spectra of Adsorbed Species, Academic Press, New York, 1966.
[9] G.M. Zhidomirov, A.V. Larin, D.N. Trubnikov, D.P. Vercauteren, J. Phys. Chem. C 113 (2009) 8258.
[10] A.V. Larin, G.M. Zhidomirov, D.N. Trubnikov, D.P. Vercauteren, J. Comput. Chem. 31 (2010) 421.
[11] A.A. Rybakov, A.V. Larin, G.M. Zhidomirov, D.N. Trubnikov, D.P. Vercauteren, Comput. Theor. Chem. 964 (2011) 108.
[12] M.J. Frisch, G.W. Trucks, H.B. Schlegel, G.E. Scuseria, M.A. Robb, J.R. Cheeseman, J.A. Montgomery Jr., T. Vreven, K.N. Kudin, J.C. Burant, J.M. Millam, S.S. Iyengar, J. Tomasi, V. Barone, B. Mennucci, M. Cossi, G. Scalmani, N. Rega, G.A. Petersson, H. Nakatsuji, M. Hada, M. Ehara, K. Toyota, R. Fukuda, J. Hasegawa, M. Ishida, T. Nakajima, Y. Honda, O. Kitao, H. Nakai, M. Klene, X. Li, J.E. Knox, H.P. Hratchian, J.B. Cross, V. Bakken, C. Adamo, J. Jaramillo, R. Gomperts, R.E. Stratmann, O. Yazyev, A.J. Austin, R. Cammi, C. Pomelli, J.W. Ochterski, P.Y. Ayala, K. Morokuma, G.A. Voth, P. Salvador, J.J. Dannenberg, V.G. Zakrzewski, S. Dapprich, A.D. Daniels, M.C. Strain, O. Farkas, D.K. Malick, A.D. Rabuck, K. Raghavachari, J.B. Foresman, J.V. Ortiz, Q. Cui, A.G. Baboul, S. Clifford, J. Cioslowski, B.B. Stefanov, G. Liu, A. Liashenko, P. Piskorz, I. Komaromi, R.L. Martin, D.J. Fox, T. Keith, M.A. Al-Laham, C.Y. Peng, A. Nanayakkara, M. Challacombe, P.M.W. Gill, B. Johnson, W. Chen, M.W. Wong, C. Gonzalez, J.A. Pople, Gaussian 03, Revision C.02, Gaussian, Inc., Wallingford, CT, 2004.
[13] (a) G. Kresse, J. Hafner, Phys. Rev. B 47 (1993) 558;
(b) G. Kresse, J. Furthmüller, Phys. Rev. B 54 (1996) 11169.
[14] G. Kresse, J. Joubert, Phys. Rev. B 59 (1999) 1758.
[15] (a) J.P. Perdew, J.A. Chevary, S.H. Vosko, K.A. Jackson, M.R. Pederson, D.J. Singh, C. Fiolhais, Phys. Rev. B 46 (1992) 6671;
(b) J.P. Perdew, K. Burke, M. Ernzerhof, Phys. Rev. Lett. 77 (1996) 3865.
[16] P. Ugliengo, D. Viterbo, G. Chiari, Z. Kristall. 207 (1993) 9.
[17] E. Garrone, B. Bonelli, C. Lamberti, B. Civalleri, M. Rocchia, P. Roy, C. Otero Areán, J. Chem. Phys. 117 (2002) 10274.
[18] N.D. Parkyns, J. Chem. Soc. A (1969) 410.
[19] A. Brunet-Bruneau, D. Souche, S. Fisson, V. Nguyen Van, G. Vuye, F. Abeles, J. Rivory, J. Vac. Sci. Technol. A 16 (1998) 2281.
[20] Q.L. Liu, A. Mace, Z. Bacsik, J.L. Sun, A. Laaksonen, N. Hedin, Chem. Commun. 46 (2010) 4502.
[21] H.A. Aleksandrov, G.N. Vayssilov, N. Rösch, J. Mol. Catal. A 256 (2006) 149.
[22] R.F.W. Bader, Atoms in Molecules: A Quantum Theory; The International Series of Monographs in Chemistry, Clarendon Press, Oxford, UK, 1995.
[23] A.V. Larin, A. Mace, A.A. Rybakov, Z. Bacsik, N. Hedin, A. Laaksonen, in preparation.
[24] N. Rane, A.R. Overweg, V.B. Kazansky, R.A. van Santen, E.J.M. Hensen, J. Catal. 239 (2006) 478.
[25] D.F. Plant, G. Maurin, H. Jobic, P.L. Llewellyn, J. Phys. Chem. B 110 (2006) 14372.
[26] T. Montanari, G. Busca, Vib. Spectrosc. 46 (2008) 45.
[27] A.V. Larin, A.A. Rybakov, G.M. Zhidomirov, A. Mace, A. Laaksonen, D.P. Vercauteren, Theoretical modeling of carbonate formation in dehydrated alkaline earth zeolites, ACS 239th National Meeting, Division of Fuel Chemistry, San Francisco, CA, USA, 21-25.3.2010, ID 26896.
[28] O.V. Udalova, E.V. Khaula, M.Y. Bykhovskii, Y.N. Rufov, A.N. Romanov, Russ. J. Phys. Chem. 77 (2003) 912.
[29] X. Huang, T.J. Lee, J. Chem. Phys. 129 (2008) 044312.
[30] J. Xu, B.L. Mojet, J.G. van Ommen, L. Lefferts, J. Phys. Chem. B 109 (2005) 18361.
[31] E.A. Pidko, E.J.M. Hensen, G.M. Zhidomirov, R.A. van Santen, J. Catal. 255 (2008) 139.
[32] G. Rebmann, V. Keller, M.J. Ledoux, N. Keller, Green Chem. 10 (2008) 207.